An experimental and numerical study on the generation of wheel-rail stick–slip contact behaviour

Zhang, Pan; Krishnan, Gokul; Yang, Zhen

DOI
10.1093/iti/liaf008

Publication date
2025

Document Version
Final published version

Published in
Intelligent Transportation Infrastructure

Citation (APA)
Zhang, P., Krishnan, G., & Yang, Z. (2025). An experimental and numerical study on the generation of wheel-rail stick–slip contact behaviour. *Intelligent Transportation Infrastructure*, *4*, Article liaf008. https://doi.org/10.1093/iti/liaf008

Intelligent Transportation Infrastructure, 2025, liaf008
https://doi.org/10.1093/iti/liaf008
Research Article

An experimental and numerical study on the generation of wheel–rail stick–slip contact behaviour

Pan Zhang, Gokul Jayasree Krishnan, Zhen Yang*

Department of Engineering Structures, Section of Railway Engineering, Delft University of Technology, Stevinweg 1, 2628 CN Delft, the Netherlands

*Corresponding author. E-mail: z.yang-1@tudelft.nl

Stick–slip is considered the root cause of railway engineering phenomena such as squeal noise and corrugation. Little consensus regarding the actual physical description of stick–slip has been achieved because its manifestations cannot be explained by a single underlying mechanism. To investigate the generation mechanisms of stick–slip contact, this study reproduced wheel–rail stick–slip experimentally with an in-house test rig—V-Track and numerically with an explicit finite element method (FEM). The V-Track is capable of reproducing realistic wheel–rail dynamic interactions under well-controlled lab conditions, while the explicit FEM has been proven to be suitable for the simulation of dynamic contact and frictional instability. Crucial influential factors including wheel–rail lateral creepage, friction levels, and friction characteristics were varied in the experiments and simulations to examine their impacts on the occurrence of stick–slip. The study shows that the creepage level needs to be sufficiently high to generate stick–slip. Stick–slip can be eliminated by reducing friction to a very low level, whereas changing the friction characteristics from negative to positive may not work for stick–slip mitigation. Moreover, wheel–rail friction conditions cannot be sufficiently represented by a single parameter, i.e. coefficient of friction.

Keywords: stick–slip; wheel–rail contact; V-Track test rig; explicit FEM; friction modifier; angle of attack.

1. Introduction

Stick–slip is described as the contact behaviour periodically alternating between adhesion and sliding with a corresponding change in the friction force (Byerlee, 1970). It has been widely observed in daily life and engineering practices. Because it has adverse effects such as severe interface deterioration, unstable vibration, and high-amplitude noise emission (Liu et al., 2023), numerous efforts have been taken to investigate its generation mechanisms and mitigation measures.

In railway applications, stick–slip contact behaviour is closely associated with the generation of squeal noise and corrugation (Rudd, 1976; Heckl and Abrahams, 2000; Eadie et al., 2002; Matsumoto et al., 2002; Pieringer, 2014; Yang and Li, 2019; Mei and Chen, 2023). Studies on the mechanisms of stick–slip have been carried out experimentally and theoretically to eliminate or mitigate stick–slip and consequent squeal noise (Rudd, 1976; Heckl and Abrahams, 2000; Pieringer, 2014; Yang and Li, 2019; Sheng et al., 2023) and corrugation (Eadie et al., 2002; Matsumoto et al., 2002; Mei and Chen, 2023). The crucial factors influencing the generation of stick–slip have been widely studied from the perspectives of friction characteristics (i.e. falling friction; Rudd, 1976) and structural system dynamics (i.e. mode coupling; Ouyang et al., 2005).

Three tentative approaches are proposed to reduce the stick–slip phenomenon (Eadie et al., 2002): (1) making the mechanical system in which the stick–slip occurs very rigid or highly damped, (2) reducing the friction between the moving surfaces to very low levels, and (3) changing the friction characteristics from negative to positive. The latter two regarding the excitation mechanism are directly related to wheel–rail frictional rolling contact behaviour, which is commonly characterized in terms of a creep curve, i.e. the functional dependence between friction force and wheel–rail creepage. The large lateral creepage between the outer leading wheel and high rail has been considered the main contributor to wheel unstable vibration and squeal (Rudd, 1976; Heckl and Abrahams, 2000). The lateral creepage is perpendicular to the wheel plane and depends on the angle of attack (AoA). The resulting lateral force then excites out-of-plane or bending oscillations of the wheel, which is very efficient for sound radiation. However, little consensus regarding the actual physical description of stick–slip has been achieved because its manifestations cannot be explained by a single underlying mechanism. For instance, the squeal phenomenon is often characterized as 'enigmatic' or 'erratic' (Vincent et al., 2006; Glocker et al., 2009), since real-world observations indicate that even for apparently identical conditions the squeal sometimes occurs and sometimes not, and its noise level fluctuates and the squeal wheel modes alternate (Thompson and Jones, 2000).

Aiming to provide new insights into the generation and countermeasure of wheel–rail stick–slip, this study investigates the effects of three crucial influential factors of stick–slip: lateral creepage, friction levels, and friction characteristics. Wheel–rail stick–slip was first reproduced experimentally with an in-house test rig—V-Track (Naeimi et al., 2018; Zhang and Li, 2023) and numerically with an explicit finite element model (Yang et al., 2019; Zhang et al., 2024). The V-Track test rig can simulate

Received: March 3, 2025. **Revised:** April 28, 2025. **Accepted:** April 29, 2025

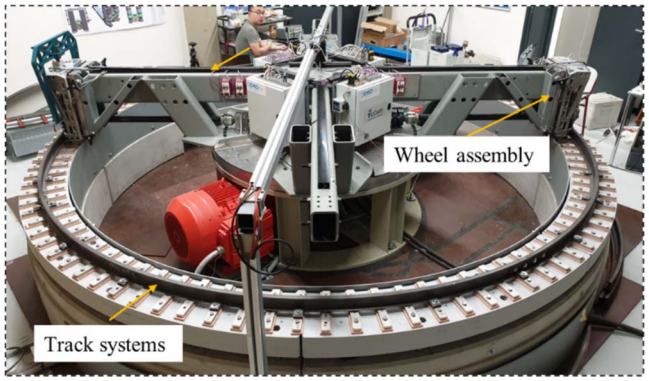

Figure 1 The structure of the V-Track test rig.

realistic wheel–rail dynamic interactions and accurately control and measure wheel–rail normal load, friction force, AoA and thus lateral creepage (Zhang et al., 2021; Yang et al., 2022) and the explicit finite element method has been proven to be suitable for the simulation of wheel–rail dynamic friction rolling contact (Yang et al., 2019; Zhang et al., 2024) and consequent phenomena such as frictional instability (Yang and Li, 2019). The wheel–rail lateral creepage level in terms of AoA, friction level in terms of coefficient of friction (COF), and friction characteristics in terms of falling (negative) or rising (positive) creep curve beyond friction saturation were then varied in both the experiments and simulations to investigate their impacts on the occurrence of stick–slip. The friction level and characteristics were changed by applying friction modifiers (FMs) in the test and predefining constant or velocity-dependent COFs in the finite element (FE) simulations. FMs have been proven effective in suppressing wheel–rail stick–slip and consequently reducing squeal noise and short pitch corrugation (Eadie et al., 2005; Eadie et al., 2008).

The structure of this paper is organized as follows. Section 2 introduces the experimental and modelling methods for studying wheel–rail stick–slip using V-Track and FE model, respectively. Section 3 presents and discusses the testing and numerical simulation results including the stick–slip generation and influential factors. The main conclusions are summarized in Section 4.

2. Methodology

2.1. Tests with the V-Track

The V-Track test facility used in this study reproduces wheel–rail frictional rolling contact under well-controlled reproducible laboratory conditions (Naeimi et al., 2018). It is approximately 1/5 scaled to the real wheel-track system and comparable to full-scale reality by considering the similarity law. As shown in Fig. 1, the V-Track consists of a maximum of four-wheel assemblies running over a ring track system with a speed of up to 40 km/h. One wheel assembly was used in the configuration of the current work to obtain the best control of the wheel–rail contact force and creepage. The wheel–rail contact force was measured in three directions with a force measurement system called a dynamometer (Zhang et al., 2021). The wheel AoA, adjustable between −2° and +2° was measured by a digital gauge mounted on the guiding block with an estimated error of approximately 6 per cent (Yang et al., 2022).

The V-Track was first run with a nominally zero-AoA at a speed of 4 km/h under the dry clean wheel–rail contact condition. The nominal wheel load was 4,500 N, producing a Hertzian contact pressure of approximately 1.2 GPa, which is representative of the contact between the wheel tread and railhead for passenger trains in the Netherlands. A braking torque of 23 N m was applied to the wheel, resulting in a longitudinal force of around 230 N. By increasing the AoA step by step, a gradual increase in the lateral wheel–rail contact force was observed as expected. Friction saturation was achieved when the AoA was over 0.4°, indicated by obvious stick–slip oscillations of the measured lateral contact force as well as the adhesion coefficient (AC) (presented in Section 3.1.1). The AC, i.e. the ratio between the magnitudes of wheel–rail friction force (the resultant of the lateral and longitudinal forces) and normal load is calculated with Equation (1).

$$\mathrm{AC} = \frac{\sqrt{F_x^2 + F_y^2}}{F_z} \tag{1}$$

where F_x, F_y, and F_z are the contact forces in the longitudinal, lateral, and vertical directions, respectively.

Then the test was repeated under the FM-conditioned conditions to investigate the influence of wheel–rail friction level and friction characteristics on stick–slip. Two types of FM, Headlub 1200 MB (hereafter Headlub for short) and Fuchs Locolub Eco (hereafter Locolub for short) were sequentially applied to the rail top surfaces with increasing dosages: from ¼ drop to ½ droplet, and then to 1 droplet of the FM. The FMs were evenly distributed over the ring track by running the V-Track for 50 cycles. For both FMs, 1 droplet weighs approximately 0.045 g (± 0.002 g). Before using the FMs, the wheel/rail interfaces were carefully cleaned with acetone and dried with a hot-air blower to guarantee comparable dry and clean contact conditions. Afterwards, a small screwdriver was used to divide the FMs of the testing dosage into very small portions and applied to the rail top.

In total eight cases were tested, as listed in Table 1. Tests 1–8, respectively, refer to the tests under the original dry clean condition, with 1/4, 1/2, and 1 droplet of Headlub per V-Track circle, dry clean test before using Locolub, with 1/4, 1/2, and 1 droplet of Locolub. By comparing the testing results of the eight testing cases, the influences of the friction level and characteristics on wheel–rail stick–slip contact behaviour can be assessed.

Table 1. Eight testing cases on the V-Track.

Dosage of the applied FMs	Headlub	Locolub
0 droplet	Test 1	Test 5
¼ droplet	Test 2	Test 6
½ droplet	Test 3	Test 7
1 droplet	Test 4	Test 8

2.2. Explicit FE wheel-track dynamic interaction model

In this study, a 3D explicit FE wheel-track interaction model of the V-Track was built up using ANSYS software, as shown in Fig. 2. The coordinate axes X, Y, and Z represent the longitudinal (rolling), lateral, and vertical directions, respectively. The wheel, rail, and sleepers were modelled as 8-node solid elements based on their real geometries and materials. The primary suspension, railpads, and ballast were modelled with spring-damper elements. The wheel–rail contact employs an automatic surface-to-surface contact scheme based on the penalty method. The track model is 3.14 m long, corresponding to one of the four rail sections. An implicit–explicit sequential approach was applied to minimize the

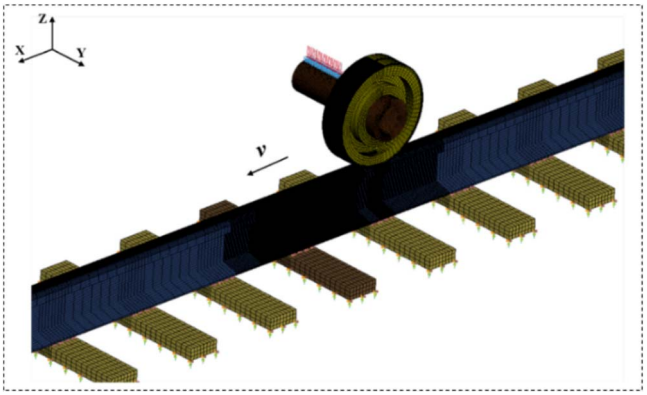

Figure 2 An explicit FE dynamin interaction model of V-Track.

Table 2. Values of parameters in the 3D FE wheel–rail model of the V-Track (Zhang et al., 2024).

Components	Parameter	Value
Wheel, rail, sleeper	Young's modulus	210 GPa
	Poisson's ratio	0.3
	Density	7,850 kg/m^3
Suspension	Vertical stiffness	230 kN/m
	Vertical damping	100 N s/m
Fastening	Vertical stiffness	290 MN/m
	Vertical damping	5.5 kN s/m
	Longitudinal stiffness	45 MN/m
	Longitudinal damping	3.4 kN s/m
	Lateral stiffness	36 MN/m
	Lateral damping	6.9 kN s/m
Rubber pad (ballast)	Vertical stiffness	17 MN/m
	Vertical damping	500 N s/m
	Longitudinal stiffness	1.5 MN/m
	Longitudinal damping	175 N s/m
	Lateral stiffness	15 MN/m
	Lateral damping	300 N s/m

computation time and the residual dynamic effects during the initialization of the wheel–rail interaction. The explicit integration time step was 15 ns, which is sufficiently small to ensure the stability of the numerical integration. The parameters of this model (see Table 2) have been calibrated and its dynamic responses in three dimensions have been validated in Zhang et al. (2024).

Nine simulation cases with different AoAs and COFs were then designed to numerically investigate the effects of creepage, friction levels, and characteristics on stick–slip, as listed in Table 3. The first set of simulations, i.e. simulation cases 1–4, aims to investigate the influence of creepage levels on stick–slip. Various lateral creepage values, approximated by AoA, were introduced to the wheel–rail interaction model by prescribing velocity boundary conditions to the wheel axle, as defined *via* Equation (2),

$$\text{Lateral creepage} = \frac{v_y}{v} \times \frac{180}{\pi} \approx \text{AoA} \tag{2}$$

where v_y is the prescribed lateral velocity of the wheel axle and v is the wheel rolling speed. The lateral creepage is approximately equivalent to AoA in radians, and can thus be converted to degrees by multiplying $180/\pi$. The simulations (cases 1–4) with AoAs of 0.2°, 0.4°, 0.8°, and 1.6° were conducted under dry clean contact conditions (COF = 0.35). Stick–slip behaviour was reproduced with an AoA of 1.6°, as presented later in Section 3.2.1.

In the second set of simulations, i.e. simulation cases 5–9, the AoA was fixed to 1.6°, and different COFs, corresponding to dry and FM-treated conditions in the V-Track tests, were applied. Among these, constant COFs were used in the simulation cases 5, 6, and 7, and velocity-dependent COFs in cases 8 and 9. The velocity-dependent COFs were defined *via* Equation (3),

$$\mu\,(v_{\text{rel}}) = \mu_d + (\mu_s - \mu_d)\, e^{-c|v_{\text{rel}}|} \tag{3}$$

where μ_s and μ_d are the static and dynamic COFs, respectively, v_{rel} is the relative sliding velocity between the wheel and the rail, and c is a decay constant that governs how rapidly the μ_s approaches the μ_d, which was taken as 6 in the FE simulations (Yang and Li, 2019). In all the nine simulation cases, a vertical wheel load of 4,500 N and a braking torque of 23 N m were applied to be aligned with the experiments.

3. Results and discussions

3.1. Test results

Both the experiment and simulation results are analysed in this section. The replications of stick–slip contact behaviour under dry contact conditions (by increasing AoAs in Test 4 and Test 8, and simulation cases 1–4) are first presented. The influences of friction conditions (with applications of different types and dosages of FMs in Tests 2–4 and 5–8) and various COFs in the simulation cases 5–9 are then analysed. The numerical contact solutions, in terms of adhesion/slip distribution within the contact patch that can indicate full or partial slip contact, are also presented. The findings from the experiment and simulation are correlated and discussed in the end.

3.1.1. *Experimental replication of stick–slip*

The time histories of the ACs measured with an increase of AoA under the original dry and clean conditions prior to using FMs (Test 1) are displayed in Fig. 3. During this test, the AoA was increased with a step of 0.08°. As expected, the measured AC increased with increasing AoA at the beginning. When the AoA was increased to 0.32°, the AC reached its upper bound of about 0.35, which can be taken as the COF under the dry contact condition. After that, stick–slip contact occurred, which can be recognized as follows: the AC increased its amplitude and the slip occurred, followed by a precipitous drop of the AC time history; and then the contact returned to the stick state until the next slip was reached with a gradual increase of AC.

The stick–slip pattern obtained in the AC results is dominated by the lateral force variation, as shown in the time history plots of the wheel–rail contact force measured with AoA = 0.4° in Fig. 4. Similar to the pattern of the AC results, the lateral wheel–rail contact force increased gradually and followed by a sudden drop in each stick–slip cycle. The drops of the lateral force correspond to the reductions of the vertical force at the time instants indicated by vertical dashed lines, while the normal load reduction is less significant. In addition, the fluctuations of the vertical and longitudinal forces, both in the wheel radial direction, share the same period (divided by the vertical dashed lines) with that of the lateral force in the wheel axle direction, indicating a mode coupling mechanism for stick–slip (Yang and Li, 2019).

Wheel–rail stick–slip was also reproduced under dry contact in Test 5 before using Locolub, as shown in Fig. 5. When comparing to the ACs displayed in Fig. 3, two differences in the wheel–rail frictional behaviour close to and during the friction saturation

Table 3. Nine simulation cases using the FE model of V-Track.

Case	COF	AoA (lateral creepage, degree)	Purposes
1	0.35	0.2	To investigate the influence of creepage levels on stick–slip
2	0.35	0.4	
3	0.35	0.8	
4	0.35	1.6	
5	0.45	1.6	To investigate the influence of friction levels and characteristics on stick–slip
6	0.20	1.6	
7	0.10	1.6	
8	0.45–0.35 (negative friction)	1.6	
9	0.25–0.35 (positive friction)	1.6	

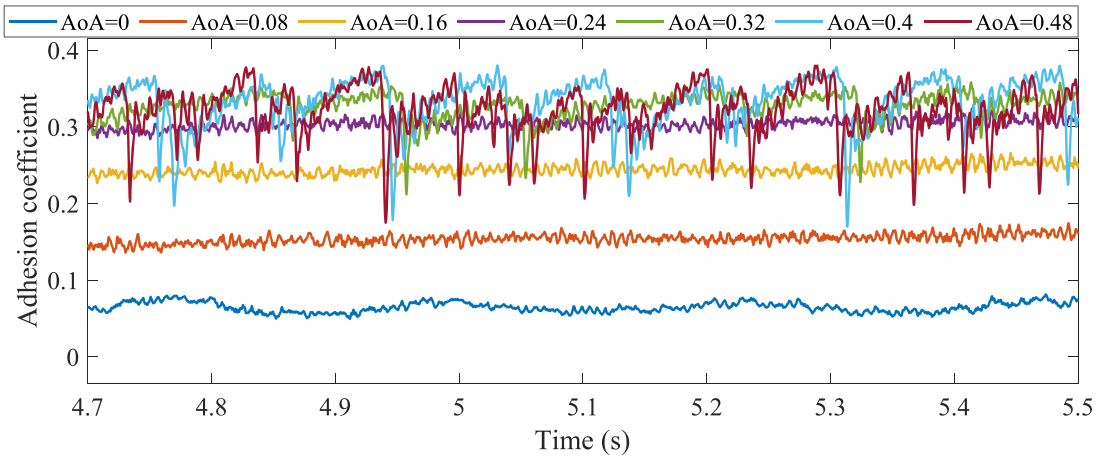

Figure 3 The time histories of the ACs measured with a range of AoAs under dry and clean conditions before using Headlub (Test 1).

are noticeable in Fig. 5, although the friction reached the level of the original dry contact condition of the V-Track (COF = 0.35) by carefully cleaning the wheel and rail interfaces after the Headlub tests. On the one hand, the intensity of the stick–slip motion in Test 1 was higher than that in Test 5: the AC dropped from 0.35 to 0.2 in Test 1 but to 0.25 in Test 5 after full slip; on the other hand, when the AoA was further increased from 0.32° to 0.48° beyond the friction saturation, a drop of friction level from 0.35 to 0.33, i.e. negative friction characteristics, was observed in Test 5, while the friction level remained in Test 1. The same COF value but different wheel–rail frictional contact behaviour observed in Test 1 and Test 5 suggest that the wheel–rail friction condition cannot be sufficiently represented by a single parameter COF. To better model the wheel–rail frictional contact, especially close to or beyond friction saturation and wheel–rail stick–slip, a more accurate representation of the wheel–rail friction condition is desirable.

3.1.2. *Influence of the tested FMs on stick–slip*

To study the influence of friction level on wheel–rail stick–slip, the time histories of the AC curves measured under eight testing conditions with friction saturation (AoA = 0.4°) are compared in Fig. 6. The measured COFs of the eight test cases are about 0.37, 0.16, 0.14, 0.12, 0.36, 0.28, 0.23, and 0.16, respectively. It is worth noticing that these measured COF values are qualitative indications of the actual wheel–rail contact situations because of the test set-up differences, as outlined in Gallardo-Hernandez and Lewis (2008), Areiza et al. (2015), and Olofsson and Lyu (2017). It can be seen that stick–slip occurred in Tests 1 and 5–7 where the COFs are higher than 0.23, while it was not observed in Tests 2–4 and Test 8 with COFs lower than 0.16. This suggests that a threshold of COF between 0.16 and 0.23 might exist which governs the occurrence of stick–slip in the V-Track configuration of that time. Stick–slip oscillations can be observed when the friction level is above this threshold, whereas reducing the COF below this value can eliminate stick–slip. This finding supports the effectiveness of the aforementioned second approach to eliminating stick–slip, i.e. reducing the friction to sufficiently low levels. However, in real-world railway applications, friction cannot be reduced too much, as maintaining an adequate friction level is critical for ensuring train braking and traction performance (Zhang et al., 2020). In addition, Fig. 6b illustrates that the application of 1/4 droplet of Locolub can reduce the friction level, but meanwhile, intensify the stick–slip oscillations. This observation aligns with the finding in Fletcher and Lewis (2013) that the use of lubricants can cause sudden drops in the AC. Therefore, the tests conducted in this study indicate that reducing the friction level, unless to a very low level below the threshold, may not always mitigate stick–slip.

Based on the ACs measured under different AoA conditions, the AC–AoA relationship, representing wheel–rail adhesion as a function of creepage, i.e. creep curve, can be obtained. The AC–AoA relationships of the V-Track influenced by FMs are presented in Fig. 7. It should be noted that the AC with zero-AoA is not zero due to the longitudinal creepage induced by the braking torque, which is not negligible (see Fig. 4). It can be seen that, as the FM dosage increases, both the adhesion level and COF decrease, and this reduction is more pronounced with Headlub compared to Locolub. In the dry contact tests (Tests 1 and 5), the AC reached the COF, i.e. friction was saturated, when AoA ≥ 0.32°, while in

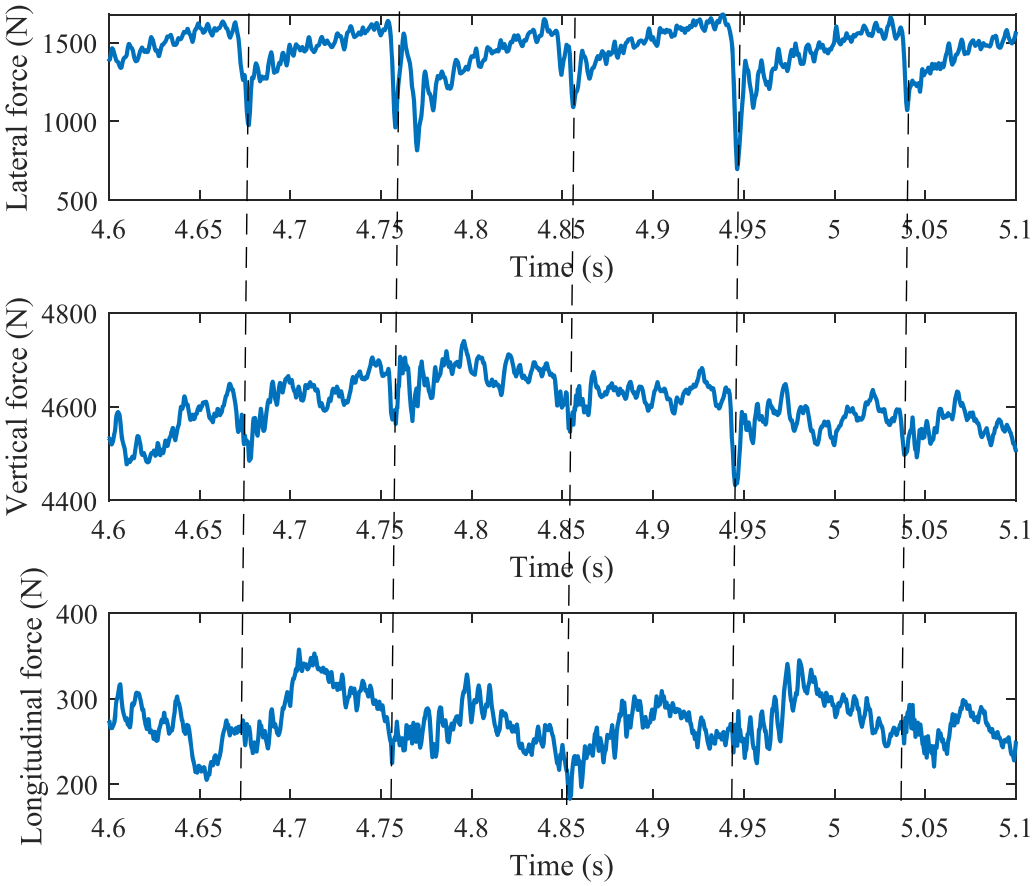

Figure 4 Measured time histories of contact forces with an AoA of 0.4° in Test 1.

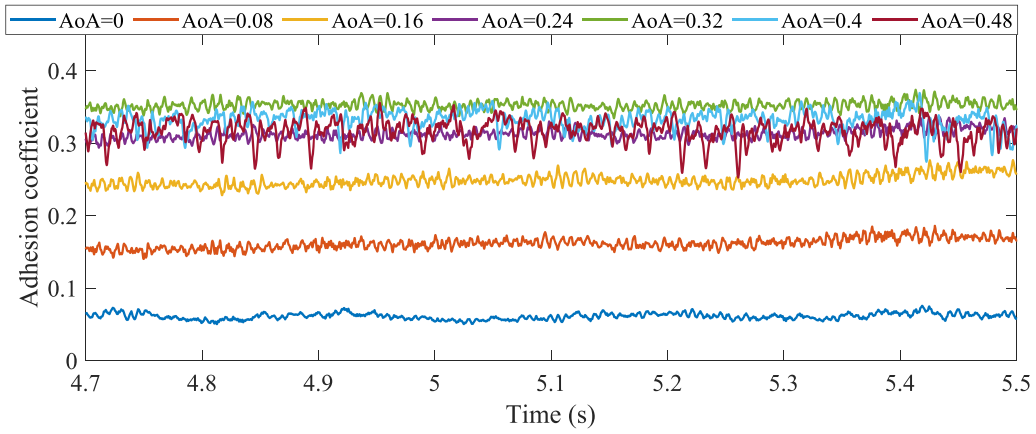

Figure 5 The time histories of the ACs measured with a range of AoAs under dry and clean conditions before using Locolub (Test 5).

the FM-treated conditions, the friction saturation was achieved with smaller AoAs: in the Headlub-treated contact tests (Tests 2–4), friction was saturated when AoA ≥ 0.16°, which can be identified by very slight increase of AC with further increase of AoA; and in the Locolub-treated contact tests (Tests 6–8), friction was saturated when AoA ≥ 0.24°, which can be identified by obvious stick–slip oscillation as dry contact.

Again, notable differences in the AC–AoA relationship beyond friction saturation were observed between the two dry clean contact tests in Fig. 7. The curve of Test 1 flattened after reaching the friction saturation point, suggesting a stable adhesion limit with constant COF. In contrast, in Test 5, a distinct drop in the creep curve was observed beyond friction saturation, indicating a 'falling friction' or 'negative friction' characteristic. The difference in COF between Test 1 and Test 5 could likely be caused by the change of rail roughness due to wear after several hundred cycles. Despite these differences in frictional behaviour, stick–slip oscillations were evident in both tests, with the phenomenon being more pronounced in Test 1. This finding suggests that falling friction characteristics are not a must for the generation of stick–slip. Instead, stick–slip can arise even under conditions where the friction coefficient remains constant (as in Test 1).

Meanwhile, it can be seen in Fig. 7 that the constant (Test 1) and negative (Test 5) friction characteristics shown in the

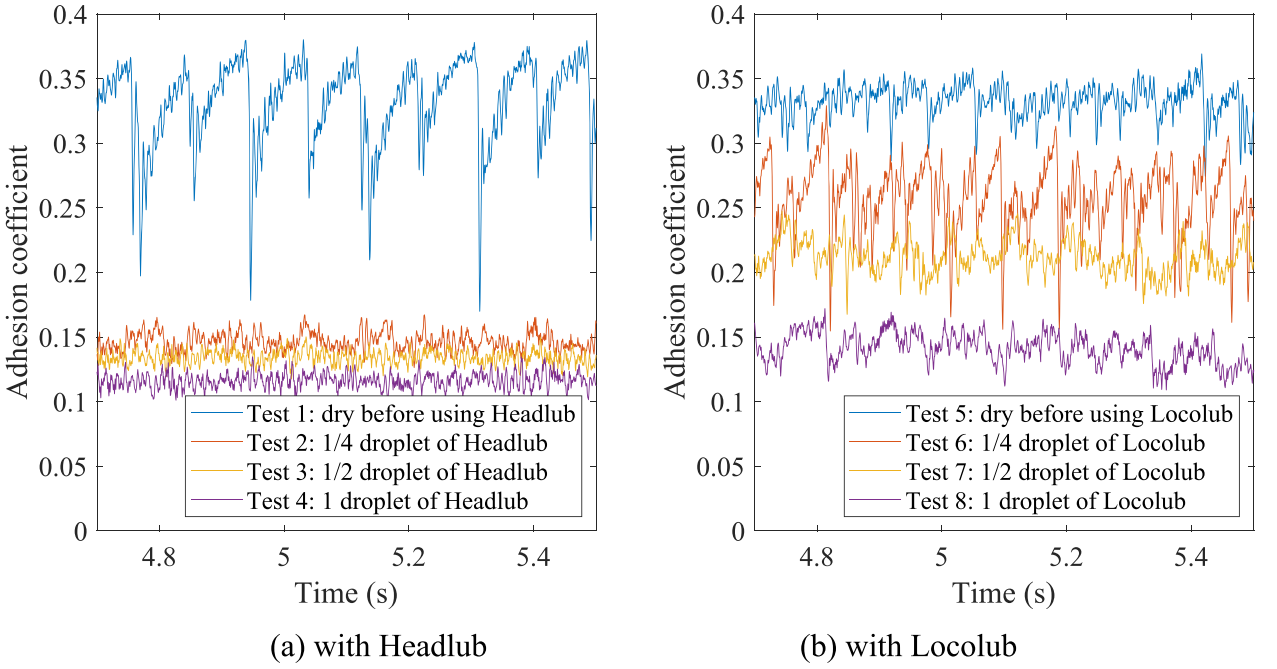

Figure 6 Influence of friction modifiers on the stick–slip.

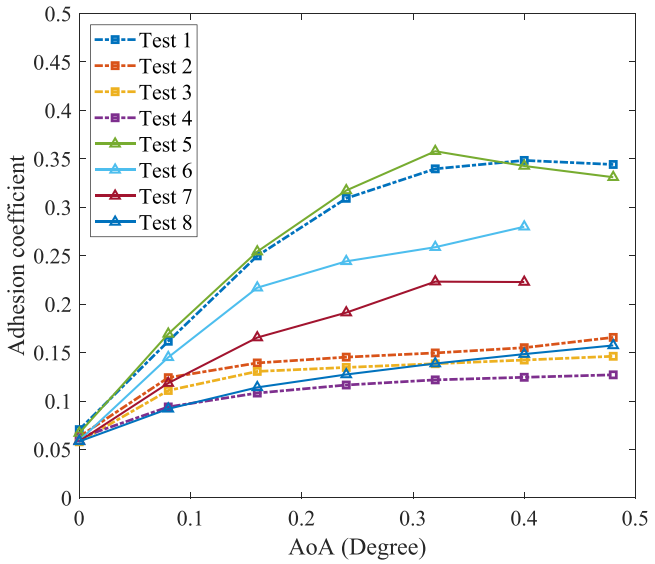

Figure 7 Influence of the FMs on the AC–AoA relationship.

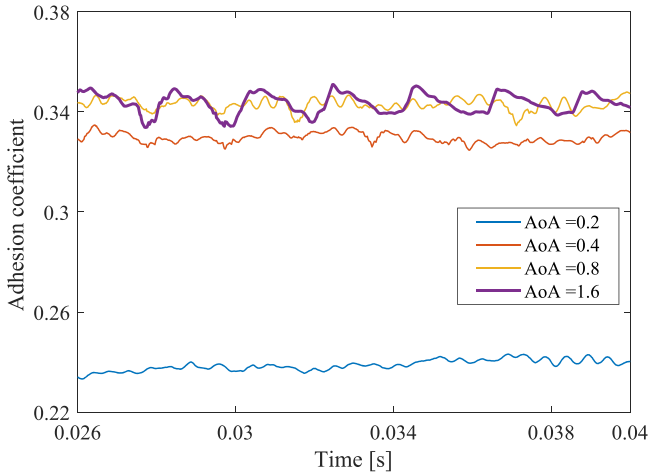

Figure 8 The time histories of the simulated ACs with the increase of AoA (simulation cases 1–4).

dry conditions were changed to positive with the applications of FMs, corresponding well to results reported in Arias-Cuevas et al. (2010), Fletcher and Lewis (2013), and Harmon and Lewis (2016). As the stick–slip was not eliminated but intensified by using Locolub despite the change of the friction characteristics to positive, we may conclude that changing the friction characteristics from negative to positive is not a sufficient condition for the reduction of stick–slip.

3.2. Simulation results

3.2.1. *Numerical replication of stick–slip*

Figure 8 presents the time histories of the simulated ACs with a constant COF of 0.35 but varies AoAs (simulation cases 1–4). Initially, a small AoA of 0.2° was applied to the FE wheel–rail contact model. At this low creepage level, the AC remained stable, and no stick–slip contact behaviour was observed. As the AoA was increased to 0.4°, 0.8° and eventually 1.6° in the simulations, a significant increase in AC was noted. Stick–slip contact behaviour was numerically reproduced when the AoA reached 1.6°, as characterized by the periodic alterations in the AC time history.

Figure 9 presents the time histories of the simulated contact forces in the lateral, vertical, and longitudinal directions with an AoA of 1.6° (simulation case 4). The lateral contact force exhibits strong fluctuations and plays a dominant role in the wheel–rail stick–slip. This is aligned with the experimental observation presented in Section 3.1. The longitudinal contact force shows similar fluctuation periodicity, as indicated by the vertical dashed lines. This phenomenon could result from the coupling between the lateral and longitudinal forces in the tangential direction, which are inherently interdependent and constrained by the frictional bound. In contrast, a weaker correlation to the vertical contact

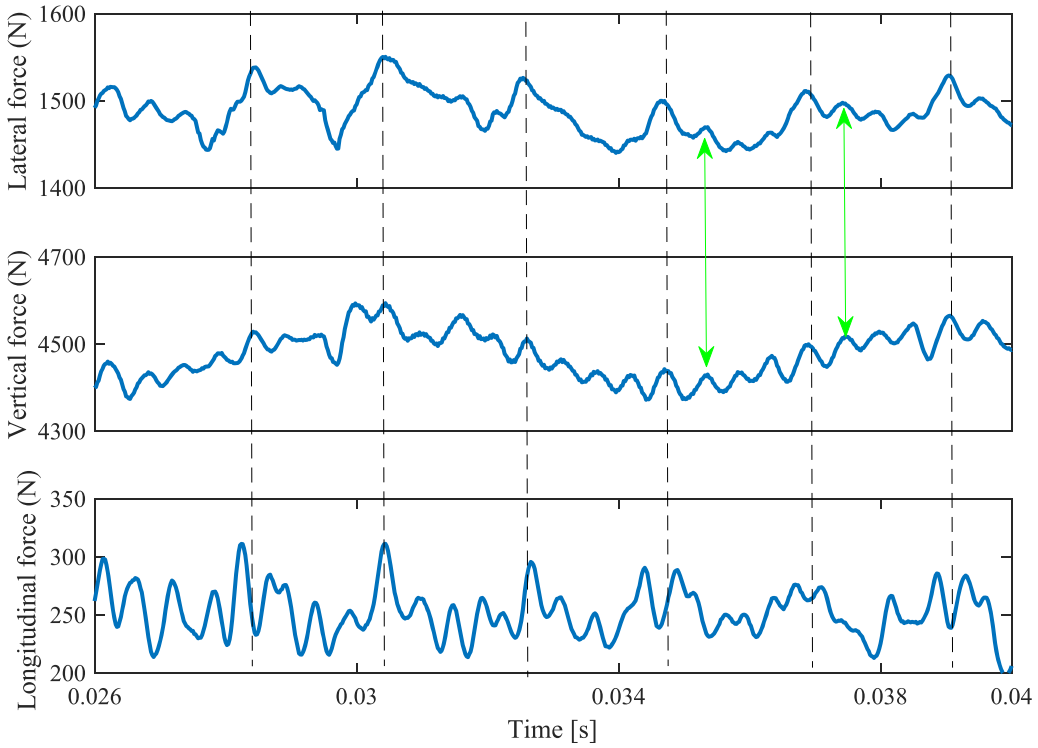

Figure 9 The time histories of simulated contact forces with an AoA of 1.6° (case 4).

force in the stick–slip periodicity is observed, while the high-frequency fluctuation in the vertical force appears to correspond well to that in the lateral force, as indicated by double arrows.

Overall, the numerically reproduced stick–slip qualitatively agrees with the test results in two aspects: (1) stick–slip contact behaviour occurred in the form of large periodical fluctuation of wheel–rail lateral force when the friction saturation was achieved by increasing the lateral creepage, or AoA and (2) during stick–slip contact, the vertical and longitudinal forces show similar periodic fluctuation pattern, indicating wheel mode coupling and friction coupling.

By comparing the wheel–rail contact surface shear stress (dashed curve) and traction bound (i.e. the production of contact pressure and COF, solid curve) in Fig. 10, the adhesion and slip regions within the contact patch can be identified. The contact region is in slip if the surface shear stress reaches traction bound, otherwise it is in adhesion. It can be seen that at $t_1 = 0.0299$ s and $t_3 = 0.0319$ s, corresponding to the dips in the AC curve shown in Fig. 10a, adhesion regions take place in the contact patch. Conversely, at the other two time instants $t_2 = 0.0305$ s and $t_4 = 0.0325$ s, corresponding to the two peaks in the AC curve, the contact patches are in full slip. These results confirm the stick–slip oscillation reproduced in the simulations, characterized by alternating phases of partial and full slip. In future work, a denser meshing scheme needs to be employed in the FE simulations to capture more accurate and detailed contact solutions (Zhao and Li, 2011).

Figure 11 corresponds the alternation of the simulated stick–slip phases to the periodical change of rail lateral motion. The vertical dashed lines indicate the locations of AC peaks, where full slip happened in the simulation. Correspondingly, we can see that the rail reached the end of one side, indicated by the dips of the displacement time history, zero velocities and maximum acceleration. After that, the rail rebounded until it moved to the other end, i.e. with the displacement rise from dips to peaks, as indicated by the solid line. In this process, the AC, as well as the wheel–rail lateral force, decreased, and when the surface shear stress was below the traction bound, the adhesion region appeared within the contact patch (see Fig. 10b and d), and the wheel and rail came back to a partial slip contact condition. After that, the AC, and wheel–rail lateral force, increased until full slip happened in the next phase. The time history of the wheel lateral acceleration generally followed the trend of AC (dominated by the wheel–rail lateral force), which is logical according to Newton's second law.

3.2.2. *Influence of friction on stick–slip*

Figure 12 compares the ACs calculated with simulation cases 4–9 (listed in Table 3) to study the influence of friction levels and characteristics on stick–slip. With a large AoA value of 1.6°, friction saturation was achieved for all simulation cases, and thus the simulated AC level increased with the applied COF value, as shown in Fig. 12a. Stick–slip occurred in the cases of COF = 0.2, 0.35, and 0.45, but not in the case of COF = 0.1. This result is consistent with the measurement finding that a threshold above 0.16 may exist which governs the occurrence of stick–slip.

To examine the influence of friction characteristics, Fig. 12b compares the AC curves obtained with constant (case 4, COF = 0.35), decreased (case 8, COF = 0.45–0.35), and increased (case 9, COF = 0.25–0.35) COFs. The decreased and increased COFs correspond to negative and positive friction characteristics, respectively. It can be seen that stick–slip was reproduced in all three simulation cases. This indicates that negative friction is not a must for stick–slip, which is also consistent with the test results presented in Fig. 6. Because friction saturation was achieved, the AC level was mainly determined by the dynamic COFs, which were equal to the constant COF of 0.35 for both velocity-dependent simulation cases.

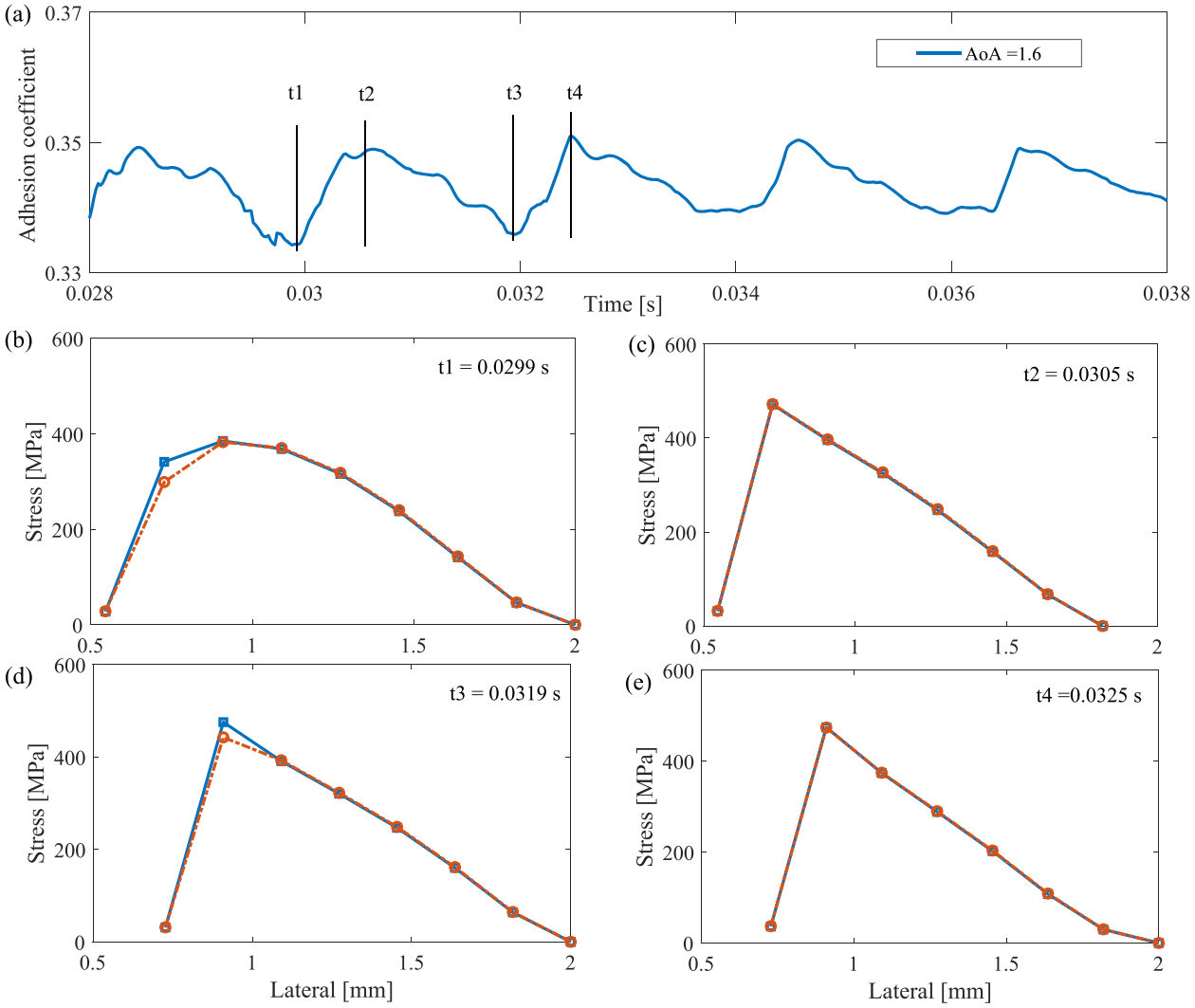

Figure 10 The simulated contact stresses at four time instants during stick–slip. (a) time history of the AC curve obtained with the simulation case 4; (b) stress distributions at $t_1 = 0.0299$ s; (c) stress distributions at $t_2 = 0.0305$ s; (d) stress distributions at $t_3 = 0.0139$ s; and (e) stress distributions at $t_4 = 0.325$ s.

3.3. Discussions on test and simulation results

Mathematically, for a single degree-of-freedom (DOF) system, negative friction is necessary to induce self-excited instability (Byerlee, 1970). However, for multiple DOF systems, the stick–slip can be induced by mode coupling with a constant COF, where the instability results from the asymmetric stiffness matrix caused by friction (Hoffmann et al., 2002). These phenomena have been reported in both railways (Pieringer, 2014; Yang and Li, 2019) and other engineering structures (Gallina and Giovagnoni, 2002). The wheel–rail systems are instinctively multiple DOF systems, and thus mode coupling is a possible explanation for wheel–rail stick–slip. The measured and simulated contact forces presented in this study, in Figs 4 and 9, respectively, suggest mode coupling in the wheel axle and radial directions.

The stick–slip reproduced in the measurements and simulations qualitatively agrees with each other in the following aspects: (1) the lateral creepage needs to be sufficiently high to induce friction saturation and then possible stick–slip oscillation; (2) there seems to be a threshold of COF (between 0.16 and 0.23 for the tests, and between 0.1 and 0.2 for the simulations), which governs the occurrence of stick–slip; (3) stick–slip can be reproduced with negative, constant, and even positive frictions; and (4) during stick–slip, the vertical and longitudinal forces show periodic fluctuation patterns similar to lateral force, possibly due to the mode coupling and friction coupling.

Differences have also been observed between the experimentally and numerically reproduced stick–slip. For instance, the measured stick–slip behaviour exhibits a low-frequency periodic pattern (e.g. around 13 Hz in Fig. 4) with a relatively small AoA of 0.6°, whereas the simulations reveal a high-frequency feature (e.g. about 500 Hz in Fig. 9) with a large AoA of 1.6°. A hypothesis can thus be proposed that the required creepage level, or AoA, for stick–slip occurrence, depends on the frequency of stick–slip oscillation. This hypothesis can be supported by the experimental results obtained from another V-Track test with different configurations, where the vertical load was 2,500 N without wheel torque, and the wheel rolling speed was 4 km/h. Figure 13 shows that when the AoA was increased to 0.54°, the low-frequency stick–slip, similar to that presented in Fig. 4, occurred with a frequency of about 15 Hz. When further increasing AoA to 1.52°,

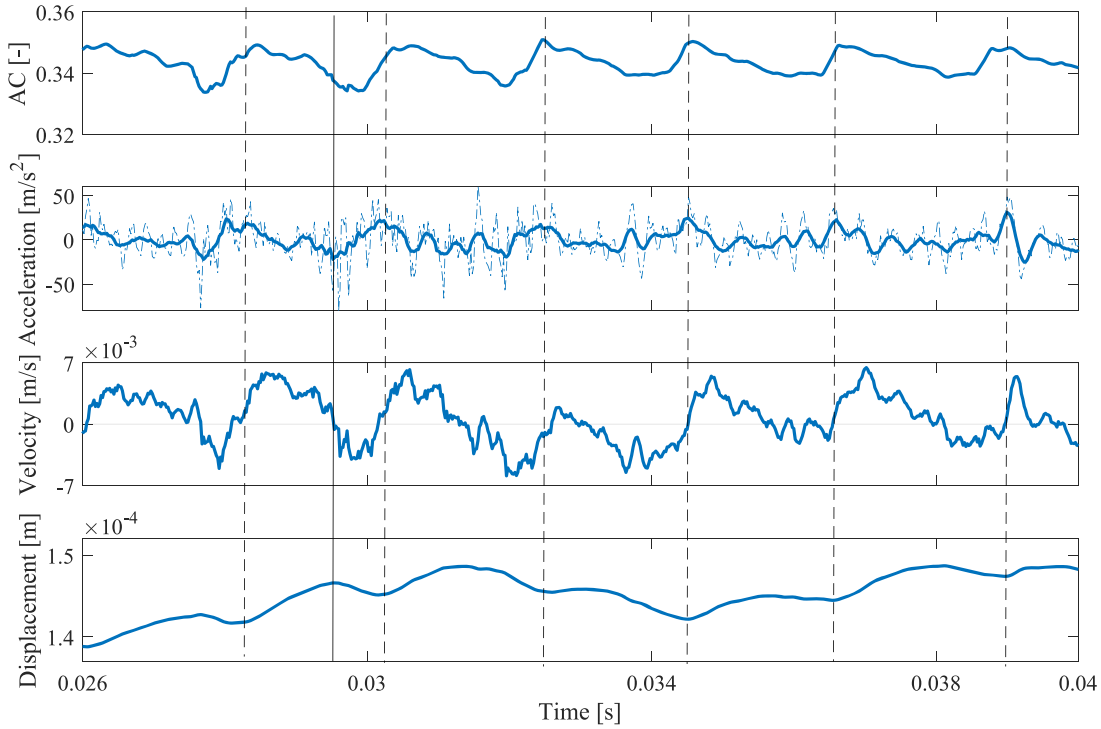

Figure 11 The correlation between the simulated stick–slip contact and rail lateral motion.

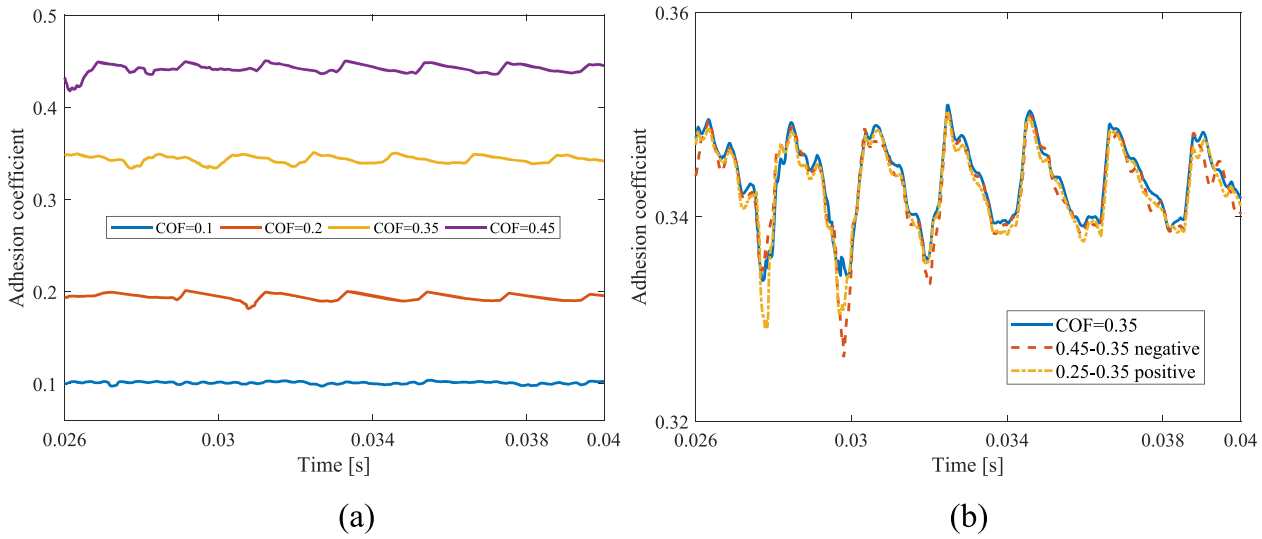

Figure 12 The influence of friction levels on stick–slip: (a) by constant COFs; (b) by velocity-dependent COFs.

the high-frequency (100 Hz) stick–slip was observed, together with a stronger low-frequency stick–slip. The low-frequency stick–slip was not replicated in the simulations of this study possibly because of the simplification of boundary conditions in the FE model. These simplifications may limit the ability of the model to capture the low-frequency dynamics of the mechanical system.

4. Conclusions

This study investigates the generation of wheel–rail stick–slip contact behaviour experimentally with the V-Track test rig, and numerically with a 3D explicit FE model. The influences of three crucial factors on stick–slip, i.e. the creepage, friction levels, and friction characteristic, are analysed by changing the AoAs, and applying FMs in the tests and different COFs in the simulations. The experimental and numerical findings qualitatively agree with each other. The main conclusions are summarized as follows.

(1) The lateral creepage must reach certain values to induce stick–slip, and the occurrence of high-frequency stick–slip requires even higher creepage: 13-Hz and 15-Hz stick–slip was reproduced in the V-Track test rig with pre-set AoAs of 0.54° and 0.6°, while 100-Hz and 500-Hz stick–slip were generated experimentally in the V-Track with an AoA of 1.52° and numerically with an AoA of 1.6°, respectively.
(2) For both measurements and simulations, there seem to be thresholds of COF (between 0.16 and 0.23 for the tests, and between 0.1 and 0.2 for the simulations), below which the stick–slip cannot be generated. Reducing friction to a very

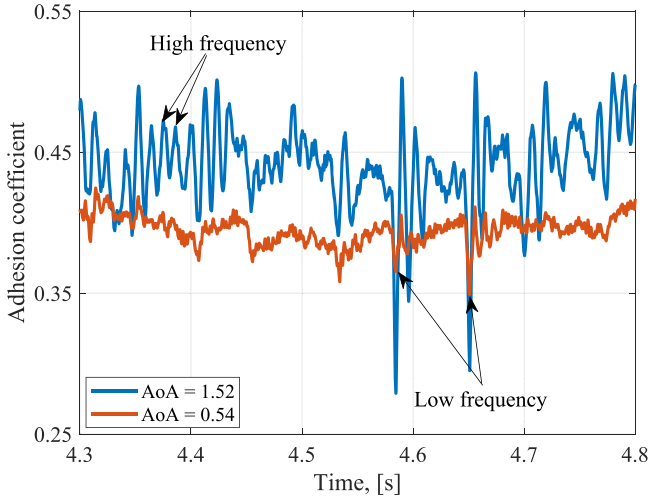

Figure 13 The correlation between the AoA and the frequency of stick–slip oscillation.

low level should thus be an effective way to eliminate stick–slip.

(3) Another tentative countermeasure against stick–slip that changes the friction characteristics from negative to positive may, however, not always work, because in both measurements and simulations, stick–slip was reproduced with negative, constant, and positive frictions.

(4) Both types of FM applied in this study can reduce the friction level and change the friction characteristics from negative to positive at the wheel–rail interface of the V-Track. Headlub effectively eliminated wheel–rail stick–slip by reducing the friction level whereas Locolub intensified wheel–rail stick–slip despite the friction characteristic being changed from negative to positive.

(5) The vertical and longitudinal forces show periodic fluctuation patterns similar to lateral force, indicating the mode coupling and friction coupling. This study reveals that the mode coupling mechanism plays a more dominant role than the falling friction mechanism in the wheel–rail stick–slip generation.

(6) Wheel–rail friction conditions cannot be sufficiently represented by a single parameter COF. To better model the wheel–rail frictional contact, especially close to or beyond friction saturation and wheel–rail stick–slip, a more accurate representation of the wheel–rail friction condition is desirable.

Acknowledgements

Parts of the study have been funded by the European Union's Horizon 2020 research and innovation programme in the project In2Track3 under grant agreement No. 101012456.

Author contributions

Pan Zhang (Conceptualization, Data curation, Formal analysis, Investigation, Methodology, Software, Validation, Visualization, Writing—original draft), Gokul Jayasree Krishnan (Data curation, Software), and Zhen Yang (Conceptualization, Data curation, Formal analysis, Investigation, Methodology, Validation, Visualization, Writing—original draft, Writing—review & editing)

Conflict of interest

None declared.

References

Areiza, Y. A. *et al.* (2015) 'Field Measurement of Coefficient of Friction in Rails Using a Hand-Pushed Tribometer', *Tribology International*, **82**: 274–279.

Arias-Cuevas, O. *et al.* (2010) 'Rolling–Sliding Laboratory Tests of Friction Modifiers in Dry and Wet Wheel–Rail Contacts', *Wear*, **268**: 543–551.

Byerlee, J. (1970) 'The Mechanics of Stick-Slip', *Tectonophysics*, **9**: 475–486.

Eadie, D. T., Kalousek, J. and Chiddick, K. C. (2002) 'The Role of High Positive Friction (HPF) Modifier in the Control of Short Pitch Corrugations and Related Phenomena', *Wear*, **253**: 185–192.

Eadie, D. T., Santoro, M. and Kalousek, J. (2005) 'Railway Noise and the Effect of Top of Rail Liquid Friction Modifiers: Changes in Sound and Vibration Spectral Distributions in Curves', *Wear*, **258**: 1148–1155.

Eadie, D. T. *et al.* (2008) 'Field Studies of the Effect of Friction Modifiers on Short Pitch Corrugation Generation in Curves', *Wear*, **265**: 1212–1221.

Fletcher, D., and Lewis, S. (2013) 'Creep Curve Measurement to Support Wear and Adhesion Modelling, Using a Continuously Variable Creep Twin Disc Machine', *Wear*, **298**: 57–65.

Gallardo-Hernandez, E. A., and Lewis, R. (2008) 'Twin Disc Assessment of Wheel/Rail Adhesion', *Wear*, **265**: 1309–1316.

Gallina, P., and Giovagnoni, M. (2002) 'Design of a Screw Jack Mechanism to Avoid Self-Excited Vibrations', *Journal of Dynamic Systems, Measurement, and Control*, **124**: 477–480.

Glocker, C., Cataldi-Spinola, E. and Leine, R. (2009) 'Curve Squealing of Trains: Measurement, Modelling and Simulation', *Journal of Sound and Vibration*, **324**: 365–386.

Harmon, M., and Lewis, R. (2016) 'Review of Top of Rail Friction Modifier Tribology', *Tribology - Materials, Surfaces & Interfaces*, **10**: 150–162.

Heckl, M. A., and Abrahams, I. (2000) 'Curve Squeal of Train Wheels, Part 1: Mathematical Model for its Generation', *Journal of Sound and Vibration*, **229**: 669–693.

Hoffmann, N. *et al.* (2002) 'A Minimal Model for Studying Properties of the Mode-Coupling Type Instability in Friction Induced Oscillations', *Mechanics Research Communications*, **29**: 197–205.

Liu, Q., Xu, L. and Feng, Q. (2023) 'Intelligent Monitoring of Vibration and Structural-Borne Noise Induced by Rail Transit', *Intelligent Transportation Infrastructure*, **2**: liad013.

Matsumoto, A. *et al.* (2002) 'Formation Mechanism and Countermeasures of Rail Corrugation on Curved Track', *Wear*, **253**: 178–184.

Mei, G., and Chen, G. (2023) 'Slip of Wheels on Rails: The Root Cause for Rail Undulant Wear', *Wear*, **523**: 204727.

Naeimi, M. *et al.* (2018) 'Development of a New Downscale Setup for Wheel-Rail Contact Experiments under Impact Loading Conditions', *Experimental Techniques*, **42**: 1–17.

Olofsson, U., and Lyu, Y. (2017) 'Open System Tribology in the Wheel–Rail Contact—a Literature Review', *Applied Mechanics Reviews*, **69**: 060803.

Ouyang, H. *et al.* (2005) 'Numerical Analysis of Automotive Disc Brake Squeal: A Review', *International Journal of Vehicle Noise and Vibration*, **1**: 207–231.

Pieringer, A. (2014) 'A Numerical Investigation of Curve Squeal in the Case of Constant Wheel/Rail Friction', *Journal of Sound and Vibration*, **333**: 4295–4313.

Rudd, M. (1976) 'Wheel/Rail Noise—Part II: Wheel Squeal', *Journal of Sound and Vibration*, **46**: 381–394.

Sheng, X. *et al.* (2023) 'Recent Advances on Research into High-Speed Railway Noise', *Intelligent Transportation Infrastructure*, **2**: liad015.

Thompson, D., and Jones, C. (2000) 'A Review of the Modelling of Wheel/Rail Noise Generation', *Journal of Sound and Vibration*, **231**: 519–536.

Vincent, N. *et al.* (2006) 'Curve Squeal of Urban Rolling Stock—Part 1: State of the Art and Field Measurements', *Journal of Sound and Vibration*, **293**: 691–700.

Yang, Z., Deng, X. and Li, Z. (2019) 'Numerical Modeling of Dynamic Frictional Rolling Contact with an Explicit Finite Element Method', *Tribology International*, **129**: 214–231.

Yang, Z., and Li, Z. (2019) 'Numerical Modeling of Wheel-Rail Squeal-Exciting Contact', *International Journal of Mechanical Sciences*, **153**: 490–499.

Yang, Z. *et al.* (2022) 'An Experimental Study on the Effects of Friction Modifiers on Wheel–Rail Dynamic Interactions with Various Angles of Attack, Railway Engineering', *Science*, **30**: 360–382.

Zhang, P. *et al.* (2024) 'Comprehensive Validation of Three-Dimensional Finite Element Modelling of Wheel-Rail High-Frequency Interaction Via the V-Track Test Rig', *Vehicle System Dynamics*, **62**: 2785–2809.

Zhang, P., and Li, Z. (2023) 'Experimental Study on the Development Mechanism of Short Pitch Corrugation Using a Downscale V-Track Test Rig', *Tribology International*, **180**: 108293.

Zhang, P., Moraal, J. and Li, Z. (2021) 'Design, Calibration and Validation of a Wheel-Rail Contact Force Measurement System in V-Track', *Measurement*, **175**: 109105.

Zhang, Z. *et al.* (2020) 'Guidance and Evaluation System for Smooth Operation of Heavy-Haul Trains', *Transportation Safety and Environment*, **2**: 226–235.

Zhao, X., and Li, Z. (2011) 'The Solution of Frictional Wheel–Rail Rolling Contact with a 3D Transient Finite Element Model: Validation and Error Analysis', *Wear*, **271**: 444–452.

Intelligent Transportation Infrastructure, 2025, liaf008
https://doi.org/10.1093/iti/liaf008
Research Article